



## Wetter or drier? Paleohydrological evidence from a 30-year resolution Holocene biomarker $\delta D$ record from Moossee, Switzerland

Maximilian Prochnow <sup>a,\*</sup>, Lisa Danius <sup>a</sup>, Paul Strobel <sup>a</sup>, Fabian Rey <sup>b</sup>, Line Rittmeier <sup>a</sup>, Michael Zech <sup>c</sup>, Willy Tinner <sup>d</sup>, Roland Zech <sup>a</sup>

<sup>a</sup> Physical Geography, Institute of Geography, Friedrich Schiller University Jena, Jena, Germany

<sup>b</sup> Geoecology, Department of Environmental Sciences, University of Basel, Basel, Switzerland

<sup>c</sup> Physical Geography, Institute of Geography, Technical University Dresden, Dresden, Germany

<sup>d</sup> Paleoecology, Department of Plant Sciences, University of Bern, Bern, Switzerland

### ARTICLE INFO

Handling editor: P Rioual

**Keywords:**

Drought  
Evapotranspiration  
Hydrological cycle  
Lipid biomarkers  
Solar forcing  
Volcanic forcing

### ABSTRACT

The hydrological cycle intensifies under global warming, causing humid areas to become wetter. However, rising temperatures also amplify seasonal ecosystem dryness, complicating the link between temperature and hydroclimate. Such divergent mechanisms challenge generalizations like 'warm and wet' in paleoclimatology on a global scale. On a regional scale, knowledge about evapotranspiration in response to past warming and cooling is still limited, but highly relevant to understand future hydroclimate. Here, we analyse the hydrogen isotope composition ( $\delta D$ ) of aquatic and terrestrial biomarkers in varved sediments from Moossee, Switzerland, covering the past 7300 years at a temporal resolution of 30 years. Based on a dual biomarker approach, we reconstruct evapotranspiration at Moossee. Our data suggests that cool and wet conditions repeatedly favored rising lake levels and advancing glaciers in the Alps but lowered treelines, e.g. at the onset of the Neoglacial, dated to ~5.5 cal ka BP. In contrast, warmer periods like the Mid Holocene or the Roman Warm Period were associated with dryness. Short-term hydrological fluctuations are partly explained by volcanic and solar forcings. Aside from an increased risk of strong convective rainfall and floods, paleohydrology provides robust evidence that an intensified hydrological cycle under global warming will substantially favor summer drought in Central Europe.

### 1. Introduction

According to the paradigm "dry gets drier and wet gets wetter" (DDWW), an intensification of the hydrological cycle due to global warming will cause an increase in moisture for wet areas, while an opposite trend to increased drought is assumed for dry regions worldwide (Held and Soden, 2006). However, the DDWW paradigm is a crude oversimplification that applies to only ~11% of the land surface area (Greve et al., 2014), and seasonal and particularly regional differences are rarely considered and remain challenging to assess (Herzschuh et al., 2022, 2023). For the Alps including their forelands and most parts of Central Europe, heavy precipitation is projected to intensify with future warming, while the risk of extreme drought and water scarcity increases as well (Kleidon, 2024; Wilhelm et al., 2022). Understanding the relationship between temperature and hydrology is thus crucial and can be improved by studying the past hydrological cycle.

Given the fact that warm air can hold more water, a common generalization in paleoclimatology is to assume 'warm and wet' versus 'cold and dry' conditions, which is of course also a crude oversimplification and needs to be questioned and evaluated regionally (Pratap and Markonis, 2022; Zech et al., 2013). For the Alps and their forelands, for instance, the available paleoclimatic evidence suggests an opposite relationship between temperature and humidity during the Holocene (e.g. Henne et al., 2018). However, this regional pattern needs to be confirmed, as high-resolution and continuous paleohydrological records are very rare. In contrast, past temperature changes are very well constrained for Central Europe and the last few thousand years. Our good understanding of the Holocene temperature history is mainly based on chironomid, treeline, tree ring and geochemical reconstructions (Büntgen et al., 2016; Heiri et al., 2015; Lang et al., 2023; Tinner and Ammann, 2001; Zander et al., 2024). Prominent examples are the Holocene Thermal Maximum (HTM, ~10 to 5 cal ka BP) (Fischer

\* Corresponding author.

E-mail address: [maximilian.prochnow@uni-jena.de](mailto:maximilian.prochnow@uni-jena.de) (M. Prochnow).

et al., 2018), the Roman Warm Period (RWP, ~2 cal ka BP), the Medieval Climate Anomaly (MCA, ~1 cal ka BP) and the Little Ice Age (LIA, ~0.5 cal ka BP) (Büntgen et al., 2016; Wanner et al., 2008). Much larger uncertainties exist regarding paleohydrology. This is partly related to the fact that hydroclimate is much more variable in space than temperature and unambiguous proxy evidence is rare. For instance, pollen-based paleoclimate reconstructions might be affected by other factors such as human impact or temperature, while for tree rings temperature may also matter (Büntgen et al., 2011; Klippe et al., 2020; Litt et al., 2009; Marquer et al., 2017; Samartin et al., 2017; Schärnweber et al., 2019). Speleothems are valuable archives to reconstruct past climate variability at a very high temporal resolution. For Central Europe, many speleothem records using stable isotope analyses ( $\delta^{18}\text{O}$ ) are available, for example the Bunker cave record in West Germany or the Spannagel cave record in the Austrian Alps (Fohlmeister et al., 2012, 2013). They provide insights particularly into Holocene temperature history and allow reconstruction of past atmospheric circulation. However, the available speleothem records reveal a high regional variability, owing to the complexity of their  $\delta^{18}\text{O}$  signal and site-specific effects, making a coherent interpretation challenging (Lechleitner et al., 2018).

Lake sediments provide detailed information about flood histories, but the amplitude of floods depends on local hydrology and can be influenced by human activities (Dwilecki et al., 2024). As a result, there seems no homogeneous pattern in Holocene flood histories across the Alps (Wilhelm et al., 2022; Wirth et al., 2013). Lake-level fluctuations were linked to solar forcing in the Western Alps (Magny, 2013). However, such relationships remain difficult to assess (Bleicher, 2013), partly because lake-level records remain spatially variable and often have only a coarse temporal resolution. Stable isotope analyses on carbonates from large pre-alpine lakes like Ammersee, where used to reconstruct the isotopic composition of lake water, which was assumed to reflect  $\delta^{18}\text{O}$  of precipitation. This is justified in view of the hydrological setting of Ammersee. However, it was shown that specific hydrological conditions between lakes and proxy seasonality can cause pronounced differences that can complicate a straightforward comparison with other hydrological reconstructions. Further, important aspects of hydrology (evaporation) and seasonality (summer versus winter) can only be revealed if different proxies and settings are considered (Grafenstein et al., 1999; Grafenstein and Labuhn, 2021; Prochnow et al., 2024b). While all those methods undoubtedly provide important paleoenvironmental information, the application of innovative proxies that can inform about specific seasonal and hydrological conditions are needed to improve our understanding of hydroclimate in the context of warming and cooling.

Compound-specific stable isotope analyses on lipid biomarkers, particularly  $\delta\text{D}$  on *n*-alkanes, have become a powerful tool for paleohydrology (Sachse et al., 2012; Zech et al., 2013). Long-chain *n*-alkanes are formed by terrestrial plants and incorporate the  $\delta\text{D}$  signal of growing season precipitation modulated by isotopic enrichment depending on the degree of leaf transpiration ( $\delta\text{D}_{\text{ter}}$ ) (Hepp et al., 2020; Kahmen et al., 2013). Short-chain *n*-alkanes derive from aquatic organisms and incorporate the isotopic composition of the lake water ( $\delta\text{D}_{\text{aq}}$ ), which is influenced by evaporative enrichment (Ficken et al., 2000; Strobel et al., 2022). Combining  $\delta\text{D}$  of long- and short-chain *n*-alkanes and investigating their isotopic differences ( $\delta\text{D}_{\text{aq}} - \delta\text{D}_{\text{ter}}$ ) in a “dual biomarker approach” (Rach et al., 2017b) has great potential and is increasingly applied (Prochnow et al., 2024a; Rach et al., 2014; Struck et al., 2022; Toney et al., 2020).

Here, we apply the dual biomarker approach to a sedimentary *n*-alkane  $\delta\text{D}$  record from Moossee in Switzerland at an outstanding temporal resolution of 30 years covering the past 7300 years. Our study aims to investigate how temperature and moisture have been interacting on a decadal scale since the Mid Holocene. We also explore possible forcings which could be responsible for such hydroclimate variations.

## 2. Materials and methods

### 2.1. Study site

Moossee is a small lake (area ~0.3 km<sup>2</sup>, max. depth ~22 m, catchment ~20 km<sup>2</sup>) located on the Swiss Plateau (47°1'17.0"N, 7°29'1.7"E, 521 m a.s.l.), 10 km north of Bern (Fig. 1a and b). The lake is fed and discharged by the small creek Urtene (Fig. 1c). Moossee is a key site for paleoenvironmental reconstructions, as its sediments are varved (from 2680 to 7064 cal a BP), very well-dated and pollen and charcoal have been analyzed, at even 10-year resolution for parts of the record (Rey et al., 2019b, 2020). The climate of the study area is influenced by dynamic low-pressure systems associated with the position of the Westerlies, bringing moisture from the Atlantic to Central Europe. Depending on the specific pressure situation, subtropical high pressure can penetrate from the Mediterranean northwards across Central Europe, causing atmospheric blocking and warm and dry conditions during summer (Fig. 1a) (Kautz et al., 2022).

### 2.2. Sampling, lipid biomarker extraction and compound-specific $\delta\text{D}$ analyses

The sediment core had been subsampled before by Fabian Rey for pollen and charcoal analyses, partly at 10-year resolution. As we aimed at a continuous 30-year resolution for our dual biomarker record, we combined samples according to the chronology of the core (Rey et al., 2019b, 2020). The age uncertainties of the deuterium dataset therefore represents the cumulative uncertainty of the combined samples.

All biomarker analyses were performed in the Biogeochemistry Lab of the Institute of Geography, Friedrich Schiller University Jena, Germany. Total lipids were extracted with dichloromethane:methanol (DCM:MeOH, 9:1) from 221 samples (~2 g dry sediment) using ultrasonic extraction. The total lipid extracts were then eluted over amino-propyl columns with DCM:2-propanol (3:1) and DCM:formic acid (98:2) to obtain the neutral and acid fractions, respectively. The neutral fractions were further separated over silicagel columns into F1 containing the *n*-alkanes (using *n*-hexane), F2 (using DCM) and F3 (using *n*-hexane: ethylacetate, 3:1). The *n*-alkane fractions were additionally cleaned over silver-nitrate and zeolite pipette columns using hexane. The zeolite traps the *n*-alkanes, then needs to be dried and dissolved in hydrofluoric acid, before the *n*-alkanes can be recovered by liquid-liquid-extraction with hexane (McDuffee et al., 2004). Although time-consuming and labor-intensive, our lab protocol yields extremely clean chromatograms and guarantees perfect peak separation for *n*-C<sub>23</sub> to *n*-C<sub>31</sub>.

The *n*-alkanes were quantified using a gas chromatograph (Agilent 7890B) equipped with an Agilent HP5MS column and a flame ionization detector (GC-FID). External *n*-alkane standards (*n*-alkane mix *n*-C<sub>21</sub> to *n*-C<sub>40</sub>; Supelco) were measured with each sequence for identification and quantification. Compound-specific  $\delta\text{D}$  was analyzed for *n*-C<sub>23</sub> to *n*-C<sub>31</sub> using an Isoprime Vision isotope ratio mass spectrometer (Elementar, Langenselbold) coupled to an Agilent 7890B gas chromatograph via a GC5 pyrolysis interface using a chromium reactor operating at 1050 °C. Helium and hydrogen were used as carrier and monitoring gases, respectively. All samples were at least measured in duplicates and yielded an analytical precision of 4.1‰ on average (standard error) and was always <11.6‰. Standard *n*-alkane mixtures (C<sub>27</sub>, C<sub>29</sub>, C<sub>31</sub>; Arndt Schimmelmann, USA) with known isotopic compositions were measured after every ten runs (*n* = 71, analytical precision <1.6‰, mean standard error 0.6‰). The isotopic values are reported in delta notation ( $\delta\text{D}$ , ‰) versus Vienna Standard Mean Ocean Water (V-SMOW). The H<sub>3</sub><sup>+</sup>-correction factor yielded stable values of 3.29 ± 0.02‰ (*n* = 16).

### 2.3. $\delta^{18}\text{O}$ and $\delta\text{D}$ analyses on lake water samples

Lake water samples from Moossee, Inkwiler See and Burgäschisee were collected in August 2024, filtered into GC-Vials using filter-

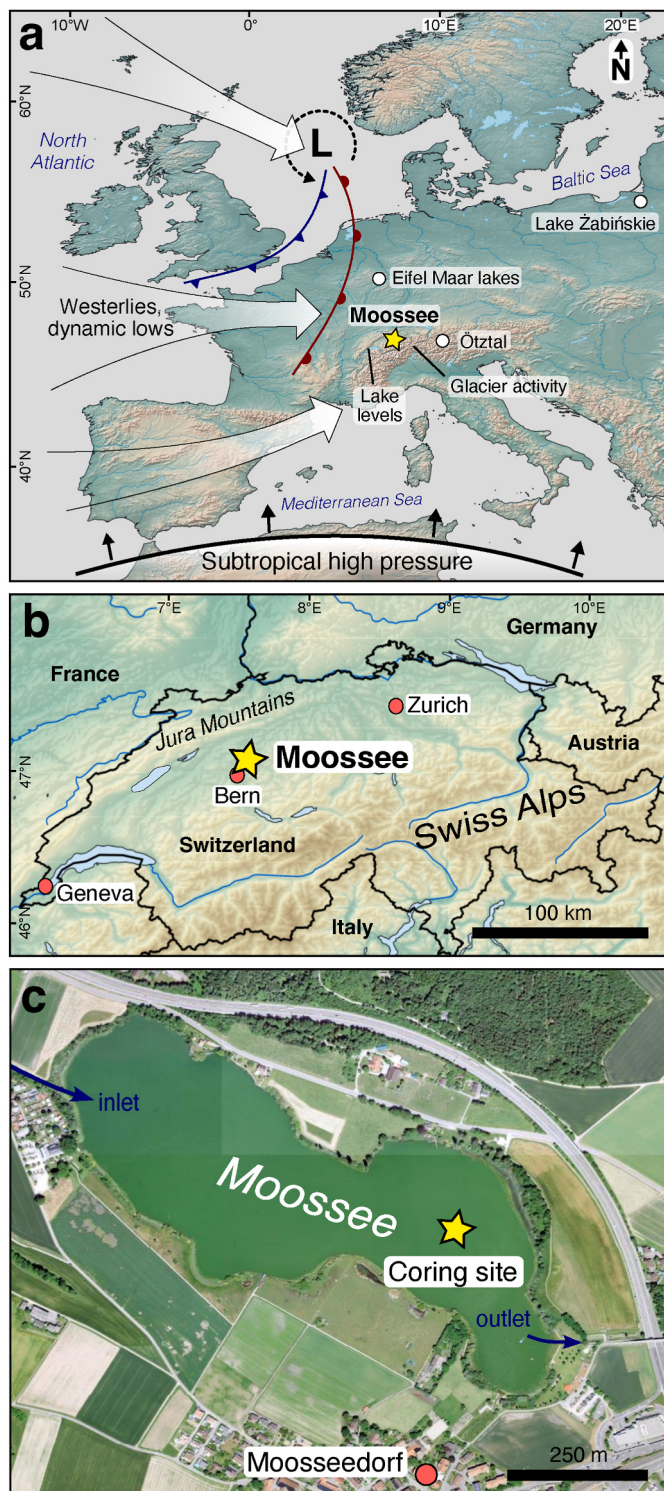


**Fig. 1.** Overview of the study area. (a) Overview of Central Europe with locations of paleorecords discussed in the text. The map indicates major atmospheric pressure features. Grey arrows represent the typical trajectories of the Westerlies and associated dynamic lows with warm (red) and cold (blue) front systems over Europe. (b) Topographic overview of Switzerland (Data: SRTM, Jarvis et al. (2008)). (c) Orthophoto of Moossee providing the coring site (modified from Rey et al. (2020); Data: [www.swisstopo.ch](http://www.swisstopo.ch)). The maps were created with SimpleMappr ([www.simplemappr.net](http://www.simplemappr.net)) and Inkscape 3.1 ([www.inkscape.org](http://www.inkscape.org)).

syringes, and stored in a fridge. The  $\delta^{18}\text{O}$  and  $\delta\text{D}$  analyses were conducted using a Picarro L2130-i Analyzer at the Core Facility Environmental Analytics at Technical University Dresden in Germany. Analytical precision of all samples was better than 0.04‰ (average 0.03‰) for  $\delta^{18}\text{O}$  and 0.2‰ (average 0.14‰) for  $\delta\text{D}$ .

## 2.4. Data handling

While each of the  $\delta\text{D}$  datapoints in this study represents a ~30 year interval, the temporal resolution of the pollen dataset from Rey et al. (2020) has a temporal resolution of 10 years between 2.7 and 7.3 cal ka BP, while the younger part has a coarser resolution. For data analyses and the vegetation correction, the tree pollen dataset was resampled to fit the mean temporal resolution of the compound-specific  $\delta\text{D}$  dataset using the QAnalyseries software (Marum Bremen). The high-resolution datasets of volcanic and solar forcings were resampled to a uniform temporal resolution (1 year). The stratospheric aerosol optical depth (SAOD) data of the HolVol database was transformed to volcanic forcing (RF) in  $\text{W m}^{-2}$  using the equation  $\text{RF} = -25 * \text{SAOD}$  given in Sigl et al. (2022). The total solar irradiance was transformed to solar forcing (SF) using the equation of Forster et al. (2007, p. 191), accounting for the ratio between the spherical surface area and the cross sectional area of the earth (0.25) as well as the planetary albedo of 0.3:  $\text{SF} = (\text{TSI} * 0.25) * 0.7$ . The resulting forcings are presented as 30-year running means.

## 3. Results and discussion

### 3.1. The terrestrial $\delta\text{D}$ and its paleohydrological interpretation

The  $\delta\text{D}$  of sedimentary lipid biomarkers, i.e. *n*-alkanes *n*-C<sub>23</sub> to *n*-C<sub>31</sub>, were measured as proxies for the isotopic composition of lake water (*n*-alkanes C<sub>23</sub> and C<sub>25</sub>) and growing season precipitation (*n*-alkane C<sub>31</sub>). The  $\delta\text{D}$  of *n*-C<sub>31</sub> ranges from -247 to -172‰ (Fig. 2a; results from all chain lengths are provided in the [Supplementary Material S1](#)). The application of the dual biomarker approach strongly depends on the source attribution of sedimentary *n*-alkanes (Hepp et al., 2019). Numerous studies investigated *n*-alkane pattern of common vegetation in Europe and confirmed that *n*-C<sub>31</sub> is mainly produced by grasses (Prochnow et al., 2024a; Schäfer et al., 2016). Deciduous trees predominantly produce *n*-C<sub>29</sub>, but also *n*-C<sub>31</sub> to a lesser degree. While grasses and deciduous trees can thus be differentiated in general, an exclusive source attribution is not possible with *n*-alkanes. Additionally, in lake sediments, aquatic organisms are also known to produce relatively large amounts of long-chain *n*-alkanes such as *n*-C<sub>27</sub> and *n*-C<sub>29</sub> (e.g. Liu and Liu, 2016). A partly aquatic contribution to *n*-C<sub>29</sub> is suggested by the correlation of  $\delta\text{D}_{n\text{-C}29}$  with  $\delta\text{D}_{n\text{-C}23}$  in our record ( $r = 0.28, p < 0.01, n = 194$ , see [Supplementary Material S1](#)). Therefore, we use *n*-C<sub>31</sub> as the most robust terrestrial endmember, which best limits the potential influence of such source overlaps.  $\delta\text{D}_{n\text{-C}31}$  is therefore dubbed as  $\delta\text{D}_{\text{terr}}$  in the following. Grasses, as the main producers of *n*-C<sub>31</sub>, are not much affected by leaf water deuterium enrichment (~15‰, Liu et al., 2017; McInerney et al., 2011; Sachse et al., 2012; Hepp et al., 2020), so its  $\delta\text{D}$  was proposed as a proxy for the isotopic composition of growing season precipitation. Due to 15‰ of leaf water deuterium enrichment and a biosynthetic fractionation ( $\varepsilon_{\text{bio}}$ ) between leaf water and leaf wax lipids of -160‰ (Sachse et al., 2012), the apparent fractionation ( $\varepsilon_{\text{app}}$ ) between precipitation and grass-derived lipids is ~ -145‰ (Hepp et al., 2020). This value is independently confirmed by other leaf wax deuterium compilations and calibrations, suggesting that the global average of  $\varepsilon_{\text{app}}$  for grasses is about -140‰ and not strongly influenced by climate (relative humidity), when no strong climate gradients (i.e. aridity) are considered. Instead, leaf wax  $\delta\text{D}$  is for the most part strongly correlated with  $\delta\text{D}$  of precipitation in these compilations (Liu et al., 2023; Liu and An, 2018, 2019; Sachse et al., 2012; Strobel et al., 2020; Struck, 2022). Similarly, Cernusak et al. (2022) found a much stronger relationship between leaf water  $\delta\text{D}$  and  $\delta\text{D}$  of atmospheric moisture

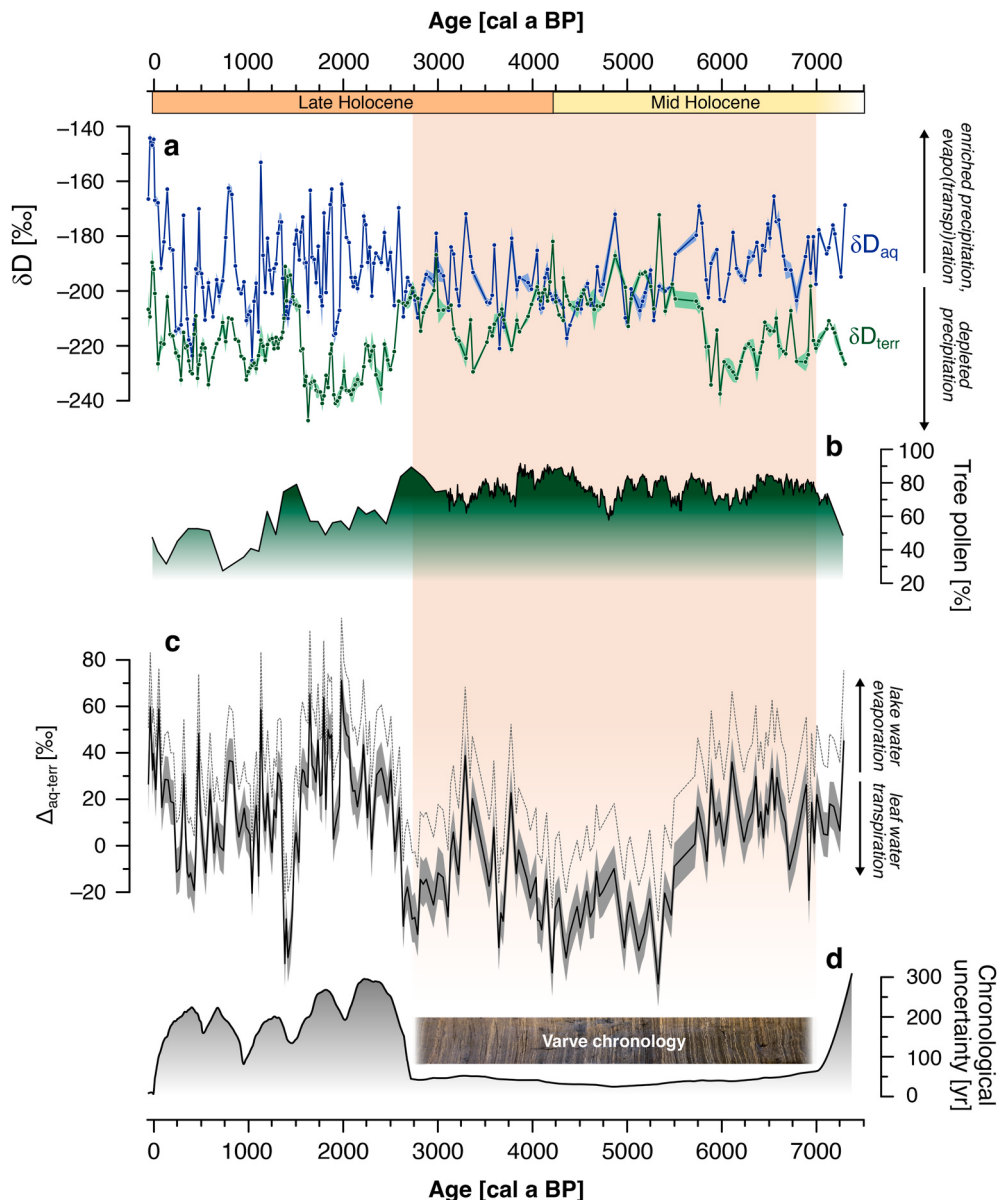


**Fig. 2.** Results of compound-specific  $\delta D$  analyses on *n*-alkanes. (a)  $\delta D_{aq}$  reflects changes in the isotopic composition of lake water based on *n*-C<sub>23</sub> and *n*-C<sub>25</sub>, and  $\delta D_{terr}$  serves as a proxy for the isotopic composition of precipitation based on *n*-C<sub>31</sub>. The blue and green ribbons indicate the analytical uncertainty expressed as standard error. (b) Moossee tree pollen used for the vegetation reconstruction (Rey et al., 2020). (c) The isotopic offset  $\Delta_{aq-terr}$  is a proxy for lake water evaporative enrichment. The dashed and black graphs show the raw and corrected  $\Delta_{aq-terr}$ . The grey ribbon represents the estimated uncertainty expressed as standard errors following error propagation. (c) Chronological uncertainty (Rey et al., 2019b, 2020). Brown shading and core photo indicate the varve chronology from 2680 to 7064 cal a BP (Photo: Fabian Rey).

(precipitation) compared to relative humidity.

While leaf water  $\delta D$  enrichment at Moossee will likely not be strongly affected by climate, vegetation changes could cause systematic differences in leaf water deuterium enrichment reflected by our  $\delta D_{terr}$ . Grasses were present at Moossee throughout the past 7300 years. However, the proportion of trees vs. grasses was variable due to deforestation and land abandonment, particularly during Roman times (~2 cal ka BP), the Dark Ages (~1.5 cal ka BP) and Medieval times (~1 cal ka BP) (Rey et al., 2020). Compared to grasses, deciduous trees show much stronger transpirative enrichment (up to ~34‰ resulting in an  $\varepsilon_{app}$  of ~−130‰) (Hepp et al., 2020; Liu and Liu, 2019; Sachse et al., 2012). Therefore, a change to 100% trees would potentially result in ~19‰ more leaf water transpirative enrichment recorded by our  $\delta D_{terr}$ . A certain influence of tree vegetation is evident when comparing  $\delta D_{terr}$  with the tree pollen record from Moossee (Fig. 2b). However, some parts of the Moossee

$\delta D_{terr}$  record exhibits more than 20‰ variability, so vegetation shifts and related transpirative enrichment alone cannot explain the observed variability in  $\delta D_{terr}$ .

When comparing Moossee  $\delta D_{terr}$  with other biomarker  $\delta D$  records from Schliersee in Bavaria, Meerfelder Maar and Holzmaar in West Germany and Lake Ghirla in the southern Alps, they all show a high magnitude of variability of more than 15‰ on multi-centennial time scales (Fig. 3a–d).

$\delta^{18}\text{O}$  of speleothems is a classic proxy to infer the isotopic signature of precipitation in Europe. The speleothem records of Bunker and Spannagel caves reveal changes in  $\delta^{18}\text{O}$  of only 1‰, which translates to ~8‰ change in  $\delta D$  (Dansgaard, 1964) (Fig. 3e–g). A comparable amplitude and long-term stability is recorded by deep water ostracod  $\delta^{18}\text{O}$  from Ammersee – a large pre-alpine lake near Munich in Bavaria (Grafenstein et al., 1996, 1999) (Fig. 3h). The registered magnitude of

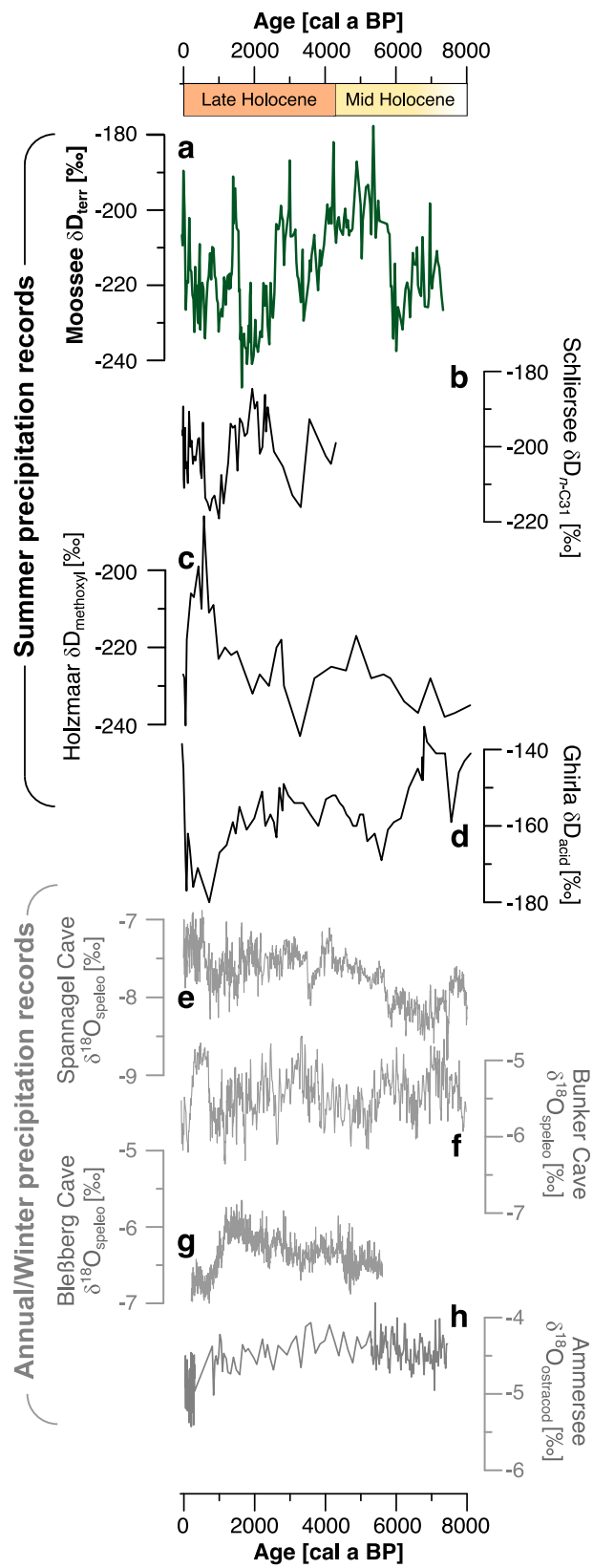


**Fig. 3.** Holocene stable isotope records for precipitation. Summer precipitation records: (a) Moossee  $\delta D_{\text{terr}}$ ; (b) Schliersee  $\delta D_{\text{terr}}$  (Prochnow et al., 2023); (c) Holzmaar  $\delta D_{\text{methoxyl}}$  (Anhäuser et al., 2015); (d) Ghirla  $\delta D_{\text{acid}}$  (Wirth and Sessions, 2016). Winter precipitation records: (e) Spannagel cave  $\delta^{18}\text{O}_{\text{speleo}}$  (Fohlmeister et al., 2013); (f) Bunker cave  $\delta^{18}\text{O}_{\text{speleo}}$  (Fohlmeister et al., 2012); (g) Bleßberg cave  $\delta^{18}\text{O}_{\text{speleo}}$  (Breitenbach et al., 2019); (h) Ammersee  $\delta^{18}\text{O}_{\text{ostracod}}$  (Grafenstein et al., 1996, 1999).

$\delta^{18}\text{O}$  changes in speleothems and Ammersee is in stark contrast to the high variability observed in the biomarker-based  $\delta D$  records and thus needs further evaluation. We hypothesize that this observed discrepancy between biomarkers, speleothems and ostracods is explained by seasonality.  $\delta^{18}\text{O}$  of Bunker and Spannagel cave integrate dominantly a winter signal due to the relatively low contribution of summer rainfall to groundwater, and the stronger influence of snow melt during spring (Fohlmeister et al., 2012). Therefore, 1‰ variability in  $\delta^{18}\text{O}$  from speleothems is explained by moisture source shifts related to the latitudinal position of the Westerlies during winter (LeGrande and Schmidt, 2006; Mangini et al., 2005; Wirth and Sessions, 2016). This is partly also true for  $\delta^{18}\text{O}$  from Ammersee due to its stable hypolimnion, large catchment and inflow originating in the northern Alps, with peak runoff during spring caused by snow and glacier melt. Its deep-water ostracod  $\delta^{18}\text{O}$  record therefore reflects a close to annual signal of precipitation, which is slightly biased towards winter (Grafenstein et al., 1996; Grafenstein and Labuhn, 2021; Prochnow et al., 2024b). This explains its relatively steady signal during the Holocene, comparable to the speleothems. Biomarker  $\delta D$  records however reflect mainly the  $\delta D$  of precipitation during the growing season (i.e. summer), and thus a direct comparison with speleothem and ostracod  $\delta^{18}\text{O}$  is not possible. During summer, the Westerlies are generally positioned more northward, whereas subtropical air masses influence weather conditions over central Europe, causing persistent atmospheric blocking and thus warm and dry conditions (Kautz et al., 2022). These conditions favor land re-evaporation and subsequent moisture recycling across Europe (Bisselink and Dolman, 2008; Sodemann and Zubler, 2010). We hypothesize that this causes a subsequent isotopic depletion of 'recycled' precipitation that is transported across Central Europe and towards the Alps and may serve as an explanation for the strong variability observed by the summer-sensitive biomarker  $\delta D$  records, which is not evident in  $\delta^{18}\text{O}$  from speleothems.

During the Mid Holocene (until 6 cal ka BP) and at around 2 and 1 cal ka BP,  $\delta D_{\text{terr}}$  is more negative at Moossee. A lower temperature gradient between the equator and the high latitudes during the warm Mid Holocene caused weaker and more northerly Westerlies, so that moisture sources were more restricted to the colder and northern polar realms, resulting in more depleted  $\delta D_{\text{terr}}$ . Moreover, this situation favored moisture recycling due to the extension of subtropical air masses. In contrast, more positive  $\delta D_{\text{terr}}$  after 5.5 and at around 2.7, 1.4 and 0.5 cal ka BP can be related to a higher temperature gradient associated with atmospheric cooling. As a result, the Westerlies were stronger and reached further south (Routson et al., 2019), providing more isotopically enriched moisture from the southern North Atlantic (LeGrande and Schmidt, 2006; Wirth and Sessions, 2016), which additionally lead to a reduced moisture recycling. The confounding effects of leaf water enrichment, seasonality and precipitation challenge a straightforward interpretation of the Moossee  $\delta D_{\text{terr}}$  in the context of other stable isotope records.

### 3.2. The aquatic $\delta D$ and its paleohydrological interpretation

The  $\delta D$  values of  $n\text{-C}_{23}$  and  $n\text{-C}_{25}$  range from  $-222$  to  $-128\text{\textperthousand}$  and from  $-229$  to  $-148\text{\textperthousand}$ , respectively, and show very similar patterns ( $r = 0.68$ ,  $p < 0.01$ ,  $n = 194$ ; see Supplementary Material S1), but do not correlate with  $\delta D_{n\text{-C}31}$  (see Supplementary Material S1), indicating different sources. Following Ficken et al. (2000), we interpret both short-chain  $n$ -alkanes to be mainly derived from aquatic plants and algae and, thus calculate and discuss their mean as  $\delta D_{\text{aq}}$  (Fig. 2a).

Compared to  $\delta D_{\text{terr}}$ ,  $\delta D_{\text{aq}}$  is on average 30‰ more positive and shows strong short-term variability. We suggest that  $\delta D_{\text{aq}}$  mainly reflects the isotopic composition of the surface lake water (i.e., the epilimnion) because aquatic productivity is strongest in the warm epilimnion in summer. Evaporative enrichment is most important during summer in the epilimnion and was reported from different lakes in Central Europe including Switzerland and Bavaria with enrichment of up to 20‰,

whereas lakes in northeastern Germany even suggest enrichment up to 30% (Aichner et al., 2021, 2022; Grafenstein and Labuhn, 2021; Ladd et al., 2018; Perini et al., 2009). This is corroborated by  $\delta^{18}\text{O}$  and  $\delta\text{D}$  of modern summer lake water from Moossee, Inkwiler See, Burgäschisee and other lakes in Switzerland (see [Supplementary Material S2](#)). Further, all Swiss and Bavarian lake water data points plot along a regional evaporation line with a slope of 5, which is very typical for temperate climates based on global compilations suggesting lake water enrichment (Horton et al., 2016; Vystavna et al., 2021).

While transpirative enrichment influences  $\delta\text{D}_{\text{terr}}$  and thus also its isotopic offset to  $\delta\text{D}_{\text{aq}}$  to some degree, the regional lake water data demonstrate that evaporative enrichment recorded by  $\delta\text{D}_{\text{aq}}$  should not be neglected a priori. Evaporative enrichment depends not only on relative humidity, but also on temperature and the radiation energy available at the lake surface (Vystavna et al., 2021). Thus, a stronger variability of lake water evaporative enrichment is likely. Under dry conditions, it is thus conceivable to expect evaporative enrichment at Moossee, considering its limited inflow from only one very small creek.

The isotopic difference between  $\delta\text{D}_{\text{aq}}$  and  $\delta\text{D}_{\text{terr}}$  ( $\Delta_{\text{aq-terr}} = \delta\text{D}_{\text{aq}} - \delta\text{D}_{\text{terr}}$ ) can thus serve as a semi-quantitative proxy for lake water evaporation versus leaf water transpiration, with more positive values indicating drier conditions and more evaporation, whereas more negative values reflect leaf water transpiration (Fig. 2b) (Strobel et al., 2022; Toney et al., 2020).

Calculating  $\Delta_{\text{aq-terr}}$  based on the raw  $\delta\text{D}_{\text{aq}}$  and  $\delta\text{D}_{\text{terr}}$  yields relative high values of sometimes >50% evaporative enrichment, which is, in view of the available lake water stable isotope data, unexpectedly high (Fig. 2c). We attribute the large magnitude of reconstructed evaporative enrichment to assumptions regarding biosynthetic fractionation of terrestrial and aquatic *n*-alkanes as well as the effects of leaf water versus lake water evaporative enrichment. Therefore, the use of raw  $\delta\text{D}_{\text{aq}}$  and  $\delta\text{D}_{\text{terr}}$  may overestimate lake water enrichment. Previously, it was assumed that the biosynthetic fractionation of aquatic and terrestrial lipids is roughly similar, i.e.  $-160\text{\textperthousand}$  (Rach et al., 2014; Sachse et al., 2012). A study by Aichner et al. (2017) investigated the fractionation between  $\delta\text{D}$  of lake water and  $\delta\text{D}_{\text{aq}}$  in *Potamogeton* in Stechlinsee, Northern Germany, and reported an aquatic  $\varepsilon_{\text{bio}}$  of only  $-136 \pm 6\text{\textperthousand}$ , which can be applied to  $\delta\text{D}_{\text{aq}}$  to calculate  $\delta\text{D}$  of lake water (eq. (1)):

$$\delta\text{D}_{\text{lake}} = ((\delta\text{D}_{\text{aq}} + 1000) / (-136\text{\textperthousand} + 1000) - 1) * 1000 \quad (1)$$

In section 3.1 we discussed the influence of vegetation on leaf water transpirative enrichment and the difference in apparent fractionation of grasses and trees. This also impacts  $\Delta_{\text{aq-terr}}$ , so it is recommended to apply the  $\varepsilon_{\text{app}}$  of grasses ( $-145 \pm 6\text{\textperthousand}$ ) on  $\delta\text{D}_{\text{terr}}$  to calculate  $\delta\text{D}$  of precipitation (eq. (2)):

$$\delta\text{D}_{\text{precip}} = ((\delta\text{D}_{\text{terr}} + 1000) / (-145\text{\textperthousand} + 1000) - 1) * 1000 \quad (2)$$

The resulting  $\delta\text{D}$  of lake water and precipitation can be used to calculate a corrected  $\Delta_{\text{aq-terr}}$  accounting for a different aquatic  $\varepsilon_{\text{bio}}$  and the  $\varepsilon_{\text{app}}$  for grasses. However, it was noted in section 3.1 that the changing abundances of grasses and trees affect the apparent fractionation between  $\delta\text{D}_{\text{terr}}$  and  $\delta\text{D}$  of precipitation by a maximum of  $\sim 19\text{\textperthousand}$ . To account for this second-order vegetation effect, we can use the high-resolution pollen data from Moossee (Fig. 2b) to estimate an additional correction factor ( $\varepsilon_{\text{corr}}$ ) after Feakins (2013) (eq. (3)):

$$\varepsilon_{\text{corr}} = f_{\text{tree}} * 19\text{\textperthousand} \quad (3)$$

This factor can be subtracted from the corrected  $\Delta_{\text{aq-terr}}$ . Such a method was successfully applied at Meerfelder Maar in West Germany (Rach et al., 2017b). The Moossee pollen reconstruction is in very good agreement with vegetation changes on the Swiss Plateau, suggesting that the tree abundances are representative for the local vegetation around Moossee (Rey et al., 2025). It should be noted that the overall temporal pattern is not affected by our correction (Fig. 2c). However, the corrected  $\Delta_{\text{aq-terr}}$  yields a considerably lower evaporative enrichment

for Moossee during the past 7300 years ( $\sim 5\text{\textperthousand}$  on average for the whole dataset, and  $\sim 17\text{\textperthousand}$  on average for the past 2000 years where the strongest enrichment occurs) compared to using raw data (Fig. 2c). Also, the overall analytical and methodological uncertainty of  $\Delta_{\text{aq-terr}}$  needs to be considered. The corrected evaporative enrichment (positive  $\Delta_{\text{aq-terr}}$ ) is well within the expectable range suggested by Central European lake water data (20–40%), whereas the transpirative enrichment (negative  $\Delta_{\text{aq-terr}}$ ) roughly agrees with reported leaf water enrichment for grasses (see discussion in section 3.1). However, the individual results should not be overinterpreted, as the uncertainties of the dual biomarker approach (apparent and biosynthetic fractionation as well as the role of leaf water enrichment) challenge a more quantitative interpretation of  $\Delta_{\text{aq-terr}}$  (see a graphical summary in [Supplementary Fig. S4](#)) and we therefore focus only on the relative pattern of  $\Delta_{\text{aq-terr}}$ . This clearly highlights the need for complementary approaches in molecular paleohydrology, such as the combination of compound-specific  $\delta\text{D}$  with additional compound-specific  $\delta^{18}\text{O}$  to further disentangle between evapo(transpi)rative enrichment and precipitation in a coupled isotope approach (e.g. Hepp et al., 2015, 2020; Lemma et al., 2021; Prochnow et al., 2023).

### 3.3. Evaporation history of Moossee based on the dual biomarker approach

The  $\Delta_{\text{aq-terr}}$  at Moossee indicates enhanced evaporation from 7.5 to 5.5 cal ka BP, from 4 to 3 cal ka BP, from 2.6 to 1.5 cal ka BP and during the last  $\sim 200$  years. Lower evaporation occurs from 5.5 to 4 cal ka BP, around 3 to 2.6 cal ka BP and after 1.4 cal ka BP with a strong variability (Figs. 3b and 4b).

Warm temperatures during the Holocene Thermal Maximum (HTM) led to enhanced evaporation at Moossee (Fig. 4a–c). This is concomitant with generally drier conditions in the region (Mauri et al., 2015; Rey et al., 2019a) and lower precipitation inferred from pollen in maar lakes in Western Germany (Litt et al., 2009).

Towards the end of the Mid Holocene 5500 to 5000 years ago, glaciers started to advance across the Alps and the treeline descended due to decreasing temperatures (Ivy-Ochs et al., 2009; Lang et al., 2023; Nicolussi et al., 2005; Solomina et al., 2015). This period is dubbed the Neoglacial, and a prominent example of cool temperatures during this time is Ötzi – the famous Neolithic ice man who died at around 5.2 cal ka BP at Tisenjoch in northern Italy (Fig. 4a). The accumulation of snow and ice due to cool temperatures during the Neoglacial conserved Ötzi until his mummy was found in 1991 CE (Ivy-Ochs et al., 2009; Kutschera and Rom, 2000). Our record provides evidence that cooler and more humid conditions favored glacial advances in the northern Alps, supported by regional lake-level high stands (Magny, 2013) and increased precipitation in Central Europe (Litt et al., 2009) (Fig. 4b–e). These circumstances prevailed until the 4.2-kyear event, which was reported to be characterized by cooler and wetter conditions in Europe (McKay et al., 2024).

During the Late Holocene, temperatures rose from 4 until 3 cal ka BP in Northeastern Europe (Zander et al., 2024), and chironomid reconstructions (Heiri et al., 2015) report a last warm phase before the Late Holocene cooling started to intensify at around 3 cal ka BP, supporting somewhat increased evaporation at Moossee. However, evaporation drops again around 2.8 cal ka BP coinciding with lower temperatures during the Göschenen/Steingletscher Oscillation (Haas et al., 1998), which is also called the Homeric Period in Central Europe. At that time, higher lake levels and glacier advances occurred in Switzerland (Magny, 2013). Wetter conditions are also indicated by diatom assemblages and geochemical proxies at Holzmaar (García et al., 2024) and a biomarker  $\delta\text{D}$  record from Meerfelder Maar (Rach et al., 2017a).

After the Homeric Period, evaporation was higher at Moossee until 1.5 cal ka BP. High-resolution tree ring reconstructions reported warmer temperatures during the Roman Warm Period at  $\sim 2$  cal ka BP (Büntgen

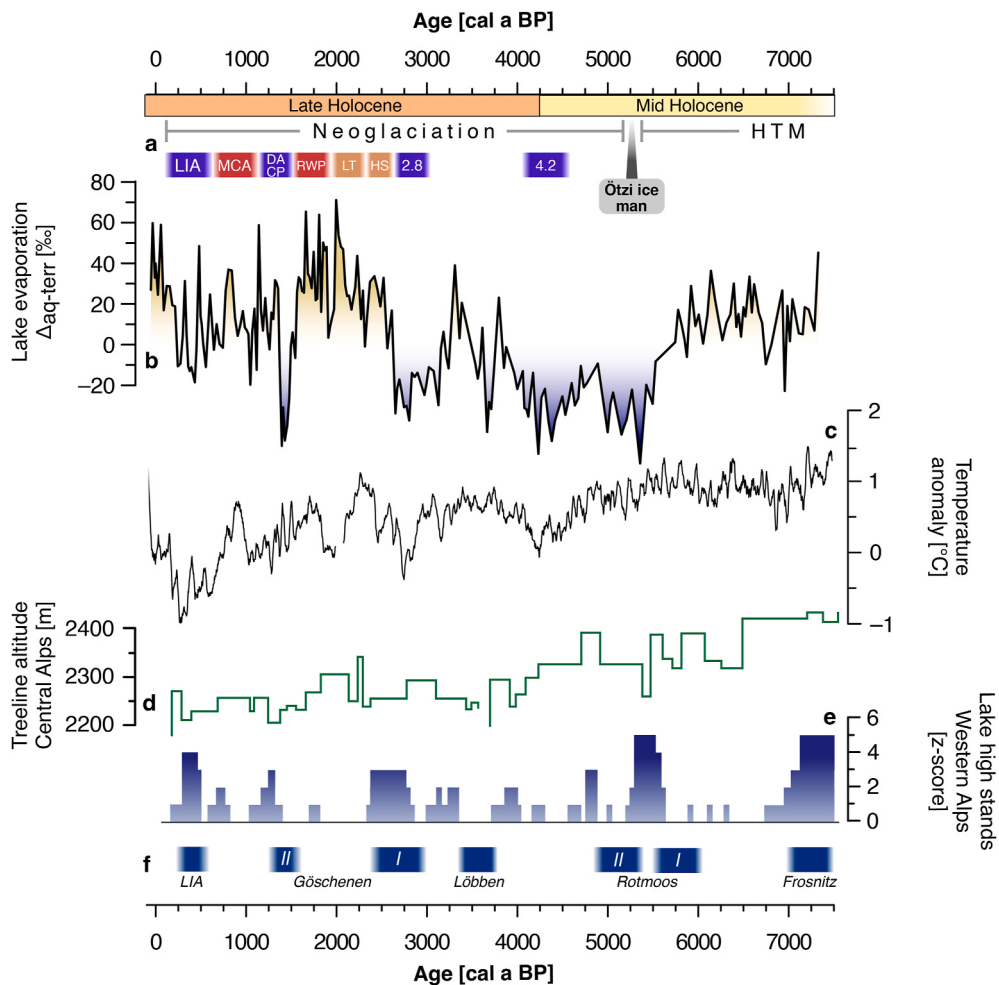


**Fig. 4.** Paleohydrological context of Moossee evaporation record. (a) Important points in climate and human history. Abbreviations correspond to those mentioned in the text. (b) Lake evaporation based on  $\Delta_{\text{aq-terr}}$  from Moossee. (c) Summer temperature reconstruction from Lake Źabińskie in Poland (Zander et al., 2024). (d) Treeline altitude in the Central Alps (Nicolussi et al., 2005). (e) Lake level high-stands in the Western Alps (Magny, 2013). (f) Glacier fluctuations in Switzerland (Ivy-Ochs et al., 2009).

et al., 2016, 2020), but interestingly, increased evaporation is visible at Moossee already before the Roman Warm Period, when salt trade started across the Alps during the Hallstatt period (~2.5 cal ka BP, HS) and later during the La Tène period (~2.2 cal ka BP, LT), when Celtic towns (*oppida*) were founded in western Switzerland (Tinner et al., 2003).

Another remarkable point in human history in Europe occurred during the migration period, which roughly corresponds with the Dark Ages Cool Period (DACP) at ~1.4 cal ka BP, where lower evaporation at Moossee, higher precipitation, advancing glaciers and higher lake levels point towards more humid conditions in concert with cooler temperatures inferred from tree rings (Büntgen et al., 2011, 2016). The Middle Ages were characterized by warmer temperatures and drier conditions in Central Europe associated with the Medieval Climate Anomaly at ~1 cal ka BP (Prochnow et al., 2024a; Scharnweber et al., 2019). Within age uncertainties, a short phase of increased evaporation at Moossee from 1.3 until 1 cal ka BP may coincide with the warm Medieval Climate Anomaly. However, evaporation remained variable, particularly towards the Little Ice Age after 1 cal ka BP. The cool Little Ice Age marks the last glacier advance in the Alps during the Holocene (Ivy-Ochs et al., 2009). This cool period was accompanied by increasing lake levels and flood activity in the Northern Alps (Wirth et al., 2013), a general trend that is valid for the entire Late Holocene (Henne et al., 2018). Thereafter, modern anthropogenic warming is recorded by stronger evaporation at Moossee.

$\Delta_{\text{aq-terr}}$  provides evidence for a relationship between temperature

and paleohydrology at Moossee. Warmer temperatures generally caused enhanced evaporation, pointing to drier conditions, which is coherent with existing paleohydrological knowledge in the region. Our dual biomarker  $\delta D$  record is unique as it is the first continuous reconstruction of its kind in a 30-year temporal resolution. With the high resolution and precise chronology of this dataset, we can explore potential forcings of the hydroclimatic variability at Moossee in detail.

#### 3.4. Volcanic and solar forcing modulates lake water evaporation

On long multi-millennial time scales, higher orbital summer insolation explains the stronger evaporation at Moossee during the Mid Holocene, while a trend to lower evaporation throughout the Late Holocene follows the decreasing summer insolation over the northern hemisphere (Laskar et al., 2004) (Fig. 5b–e). However, our high-resolution  $\Delta_{\text{aq-terr}}$  record reveals a strong centennial variability during the past 7300 years, which cannot be attributed to long-term orbital forcing. The precise age model of Moossee allows a direct comparison of our deuterium dataset with other high-resolution records of climate forcing such as total solar irradiance and global volcanic aerosol concentrations during the Holocene.

Total solar irradiance describes the variability of solar insolation due to changes in the sun's activity. Higher sun activity corresponds to more sunspots and more energy emissions resulting in  $\sim 1 \text{ W m}^{-2}$  more insolation reaching the earth's atmosphere ( $\sim 0.1 \text{ W m}^{-2}$  on the earth's

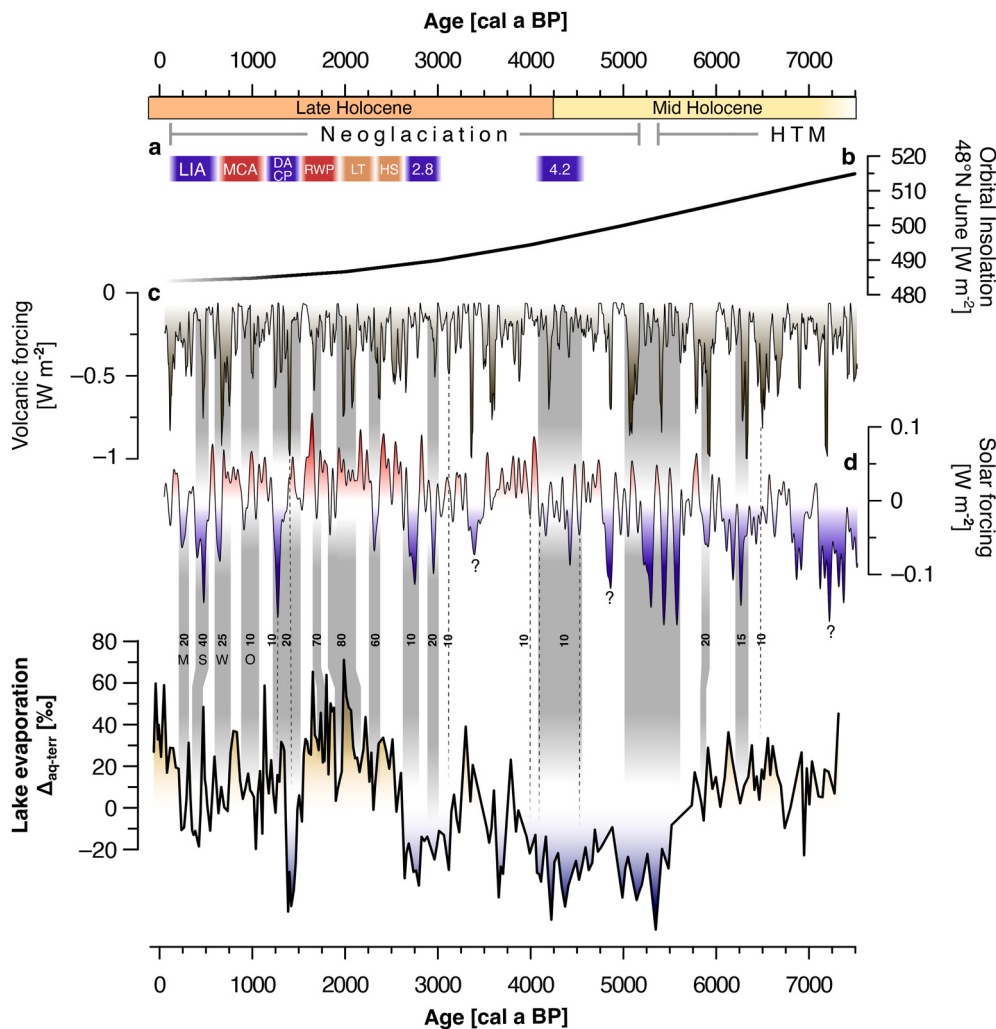


**Fig. 5.** Influence of orbital, solar and volcanic forcings on evaporation at Moossee. (a) Important points in climate and human history (abbreviations as in Fig. 3). (b) Orbital forcing for 48°N in June (Laskar et al., 2004). (c) Volcanic forcing (Sigl et al., 2022). (d) Solar forcing (Steinhilber et al., 2009). Abbreviations correspond to Maunder, Spörer, Wolf and Oort sunspot minima. (e) Lake evaporation based on  $\Delta_{\text{aq-terr}}$  from Moossee. Grey shadings indicate coincidence of low enrichment with solar or volcanic forcing with bold values indicating age differences that are within chronological uncertainties.

surface) (Forster et al., 2007). A solar irradiance reconstruction by Steinhilber et al. (2009) based on cosmogenic nuclides shows some similarities between lower solar forcing and lower evaporation at Moossee (Fig. 5d). This is particularly visible at around ~5.5 cal ka BP during a period of low solar forcing and during the Homeric Grand Solar Minima ~2.8 cal ka BP. During the last 2000 years, the Dark Age Solar Minimum and the prominent sunspot minima during the Little Ice Age called Oort, Wolf, Spörer and Maunder solar minima (Wanner et al., 2022) seem to be registered by lower evaporation (Fig. 5d and e). However, not all phases of reduced evaporation are explainable by solar forcing alone.

Strong and frequent volcanic eruptions can influence the earth's energy budget by emitting large quantities of aerosols into the troposphere, reducing the amount of short-wave radiation reaching the earth's surface. The HolVol database by Sigl et al. (2022) allows the comparison of evaporation at Moossee with global volcanic aerosol emissions and corresponding volcanic forcing during the Holocene (Fig. 5c). However, solar and volcanic forcings can amplify or weaken each other, which is why both forcings should be considered together. Both forcings show similarities with our Moossee evaporation record during the past 7300 years. Even in the younger sediments (<2.8 cal ka BP), where the chronology of Moossee has higher age uncertainties, these similarities exist, and evaporation seems to be influenced by

volcanic and solar forcings.

We can evaluate the possible link between solar and volcanic forcings and  $\Delta_{\text{aq-terr}}$  considering the age uncertainties between those records (Fig. 2d, see a detailed comparison in Supplementary Material S3). The age uncertainty for the TSI reconstruction ( $\pm 20$  years, GICC05, Vinther et al. (2006)) and the HolVol database ( $\pm 20$  years, Sigl et al. (2022)) is comparable to the varved section of the Moossee record from 2.7 to 7 cal ka BP ( $\pm 35$  years, Rey et al. (2019b)). Overlaps between minima in  $\Delta_{\text{aq-terr}}$  and volcanic or/solar forcings are mostly within the age-uncertainty of all three records (bold values in Fig. 5 and Supplementary Material S3). Around the 4.2-kyr event and the onset of the Neoglacial at 5.5 cal ka BP, cluster of lower solar and high volcanic activities generally agree with low evaporation at Moossee. Solar and volcanic forcings are highly variable at those times, but our sampling resolution is too low in this section and potential overlaps lie just outside the chronological uncertainty of Moossee. Other pronounced minima in radiative forcing do not appear to have a directly corresponding minimum in  $\Delta_{\text{aq-terr}}$  (3.4, 4.8 and 7.4 cal ka BP). A possible mechanism explaining the relationship between volcanic and solar forcings and evaporation could be as follows: due to higher insolation controlled by solar and volcanic activities, more energy reaching the earth's surface leads to higher temperatures as well as more evaporation, favoring higher evaporative enrichment of lake water. However, at the moment,

it is not possible to quantify the influence of radiation changes on evaporative enrichment, as evaporation and its isotope fractionation processes are not only dependent on radiation energy and air temperature. They are also influenced by the relative humidity of the atmosphere, sensitive heat and wind (Vystavna et al., 2021), which might be a reason why not all changes in radiative forcing are recorded by  $\Delta_{\text{aq-terr}}$ .

Nonetheless, the influence of solar and particular volcanic forcing on temperatures is known from several studies, for example, tree-ring reconstructions (Büntgen et al., 2016, 2020). A relationship between solar forcing and lake level fluctuations was suggested by Magny (2013), though this interpretation was also questioned (Bleicher, 2013). More recently, other Late Glacial and Holocene biomarker stable isotope studies discovered a connection between solar forcing and hydrology (Hepp et al., 2019; Mekhaldi et al., 2020; Prochnow et al., 2024a, 2024b). Our Moossee biomarker δD record adds confidence to these earlier results continuously for the Mid and Late Holocene at a high temporal resolution and with a precise age control.

In addition to solar and volcanic forcings, changes in the atmospheric circulation could also influence the hydrological conditions at Moossee – as discussed above for  $\delta D_{\text{terr}}$ . When the temperature gradient between the equator and high latitudes is weak, subtropical high-pressure might penetrate towards the north, causing atmospheric blocking and hence dry conditions across Central Europe. This explains higher  $\Delta_{\text{aq-terr}}$  during the warmer Mid Holocene, Roman Warm Period and Medieval Climate Anomaly. In contrast, a strong temperature gradient due to cooler temperatures after 5.5 cal ka BP, during the Homeric Period (2.7 cal ka BP), the Dark Ages Cool Period (1.5 cal ka BP) and during the Little Ice Age (0.5 cal ka BP) intensifies moisture transport by the Westerlies, resulting in a wet climate reflected by lower  $\Delta_{\text{aq-terr}}$ . Several previous studies discuss a relationship between hydroclimate and the mode of the North Atlantic Oscillation (NAO) (Adolph et al., 2024; Breitenbach et al., 2019; Faust et al., 2016; Olsen et al., 2012). The NAO is a climate pattern shifting between a positive and negative mode on a multi-annual to decadal time scale. During a positive NAO, the Westerlies are generally further north bringing moisture to North Europe, whereas the Mediterranean is drier and vice versa. While the NAO is indeed influencing Switzerland, it needs to be considered that this atmospheric mechanism is a winter phenomenon while lipid biomarker reconstructions are summer-sensitive (see discussion in section 3.1 and Wirth and Sessions (2016) and Prochnow et al. (2024a)).

#### 4. Wetter or drier? Concluding remarks

Our high-resolution δD record from Moossee shows that warmer periods were repeatedly characterized by more evaporation and thus drier conditions. On the other hand, cooler periods coincided with reduced evaporation, pointing towards more humid conditions. Hence, the Moossee record, and other proxy data discussed do not confirm the general climatological notion of warmer and wetter, as assumed particularly with the “dry gets drier and wet gets wetter”-paradigm for humid areas globally. Caution should therefore be exercised when hydroclimatic generalizations are used to contextualize proxy data or to evaluate future hydroclimatic variability. The different sensitivity of proxies to temperature and humidity, seasonality as well as regional heterogeneity (Herzschuh et al., 2023) should always be considered for the interpretation of paleorecords and the development of climate compilations. The Moossee biomarker δD record highlights the importance of molecular paleohydrology to understand the hydroclimate evolution on different time scales. Further, it demonstrates the great advantage of precisely dated, high-resolution paleoclimate records to explore and investigate relationships between archives, proxies and forcings. However, applying the dual biomarker approach comes with uncertainties regarding the degree of leaf versus lake water enrichment and the influence of changing vegetation and apparent fractionation on

terrestrial  $\delta D_{\text{n-alkane}}$ . Thus both leaf and lake water enrichment should be considered. Amending such biomarker δD records with for example complementary biomarker  $\delta^{18}\text{O}$  analyses might help to overcome these methodological challenges in molecular paleohydrology (Lemma et al., 2021; Prochnow et al., 2024b; Tuthorn et al., 2014).

Nonetheless, our data provides confirmation from the past for existing projections for the Alps and Switzerland, suggesting that severe summer droughts (Scherrer et al., 2022) and increased evapotranspiration are more likely to occur with anthropogenic warming. Additionally, more heat and evaporation over land will likely increase the risk of strong convective rainfalls, hence leading to a higher risk of local flood events across the Alps (Giorgi et al., 2016; Kleidon, 2024; Wilhelm et al., 2022).

#### Credit author contributions statement

Maximilian Prochnow: Writing – original draft, Writing – review & editing, Conceptualization, Methodology, Investigation, Formal analysis, Data curation, Visualization, Funding acquisition, Project administration.

Lisa Danius: Writing – review & editing, Conceptualization, Investigation, Visualization.

Paul Strobel: Writing – review & editing, Supervision, Methodology, Investigation, Data curation, Validation.

Fabian Rey: Writing – review & editing, Resources, Validation, Investigation.

Line Rittmeier: Writing – review & editing, Investigation.

Michael Zech: Writing – review & editing, Resources, Validation, Investigation.

Willy Tinner: Writing – review & editing, Resources, Validation, Investigation.

Roland Zech: Writing – review & editing, Conceptualization, Supervision, Resources, Investigation, Project administration.

#### Declaration of competing interest

The authors declare that they have no known competing financial interests or personal relationships that could have appeared to influence the work reported in this paper.

#### Acknowledgements

This study is funded by the German Research Foundation (DFG grant no. 538367707, ZE-860/10-1). Maximilian Prochnow gratefully acknowledges funding by a scholarship of the federal state of Thuringia (Landesgraduiertenstipendium). Oliver Heiri (University Basel) is thanked for his support improving and modelling the final chronology of Moossee. Alexander Brenning (FSU Jena) and Anthony Romano (University of Melbourne) provided feedback on statistical analyses of the data. Diana Burghardt (TU Dresden) carried out lake water stable isotope analyses. Marcel Bliedtner and Janik Wulf are thanked for their assistance during isotope measurements. The authors thank the Editor Patrick Rioual, Paul Zander and another anonymous reviewer for their critical thoughts and helpful suggestions that improved this manuscript.

#### Appendix A. Supplementary data

Supplementary data to this article can be found online at <https://doi.org/10.1016/j.quascirev.2025.109602>.

#### Data availability

The datasets generated during the current study are available in the [Supplementary Material](#) of this article.

## References

- Adolph, M.L., Czerwiński, S., Dreßler, M., Strobel, P., Bliedtner, M., Lorenz, S., Debreit, M., Haberzettl, T., 2024. North Atlantic Oscillation polarity during the past 3000 years derived from sediments of a large lowland lake, Schweriner See, in NE Germany. *Clim. Past* 20, 2143–2165. <https://doi.org/10.5194/cp-20-2143-2024>.
- Aichner, B., Dubbert, D., Kiel, C., Kohnert, K., Ogashawara, I., Jechow, A., Hilt, S., 2021. Water isotope values from northeastern German lake systems 2020 et seq. PANGAEA. <https://doi.org/10.1594/PANGAEA.935633>.
- Aichner, B., Dubbert, D., Kiel, C., Kohnert, K., Ogashawara, I., Jechow, A., Harpenslager, S.F., Höcker, F., Nejstgaard, J.C., Grossart, H.P., Singer, G., Wollrab, S., Berger, S.A., 2022. Spatial and seasonal patterns of water isotopes in northeastern German lakes. *Earth Syst. Sci. Data* 14, 1857–1867. <https://doi.org/10.5194/essd-14-1857-2022>.
- Aichner, B., Hilt, S., Périllon, C., Gillefalk, M., Sachse, D., 2017. Biosynthetic hydrogen isotopic fractionation factors during lipid synthesis in submerged aquatic macrophytes: effect of groundwater discharge and salinity. *Org. Geochem.* 113, 10–16. <https://doi.org/10.1016/j.orggeochem.2017.07.021>.
- Bisselink, B., Dolman, A.J., 2008. Precipitation recycling: moisture sources over Europe using ERA-40 data. *J. Hydrometeorol.* 9, 1073–1083. <https://doi.org/10.1175/2008JHM962.1>.
- Bleicher, N., 2013. Summed radiocarbon probability density functions cannot prove solar forcing of Central European lake-level changes. *Holocene* 23, 755–765. <https://doi.org/10.1177/0959683612467478>.
- Breitenbach, S.F.M., Plessen, B., Waltgenbach, S., Tjallingii, R., Leonhardt, J., Jochum, K.P., Meyer, H., Goswami, B., Marwan, N., Scholz, D., 2019. Holocene interaction of maritime and continental climate in Central Europe: new speleothem evidence from Central Germany. *Global Planet. Change* 176, 144–161. <https://doi.org/10.1016/j.gloplacha.2019.03.007>.
- Büntgen, U., Arseneault, B., Boucher, É., Churakova, O.V., Gennaretti, F., Crivellaro, A., Esper, J., 2020. Prominent role of volcanism in Common Era climate variability and human history. *Dendrochronologia* 64, 125757. <https://doi.org/10.1016/j.dendro.2020.125757>.
- Büntgen, U., Myglan, V.S., Ljungqvist, F.C., McCormick, M., Di Cosmo, N., Sigl, M., Jungclaus, J., Wagner, S., Krusic, P.J., Esper, J., Kaplan, J.O., de Vaa, M.A.C., Luterbacher, J., Wacker, L., Tegel, W., Kirdyanov, A.V., 2016. Cooling and societal change during the late antique Little ice age from 536 to around 660 AD. *Nat. Geosci.* 9, 231–236. <https://doi.org/10.1038/ngeo2652>.
- Büntgen, U., Tegel, W., Nicolussi, K., McCormick, M., Frank, D., Trouet, V., Kaplan, J.O., Herzig, F., Heussner, K.-U., Wanner, H., Luterbacher, J., Esper, J., 2011. 2500 Years of European climate variability and human susceptibility. *Science* 331, 578–582. <https://doi.org/10.1126/science.1197175>.
- Cernusak, L.A., Barbetta, A., Bush, R.T., Eichstaedt, R., Ferrio, J.P., Flanagan, L.B., Cuntz, M., 2022. Do  $^2\text{H}$  and  $^{18}\text{O}$  in leaf water reflect environmental drivers differently? *New Phytol.* 235, 41–51. <https://doi.org/10.1111/nph.18113>.
- Dansgaard, W., 1964. Stable isotopes in precipitation. *Tellus* 16, 436–468. <https://doi.org/10.1111/j.2153-3490.1964.tb00181.x>.
- Dwileks, A.R., Rey, F., Morlock, M.A., Glauš, N., Szidat, S., Vogel, H., Anselmetti, F.S., Heiri, O., 2024. Holocene vegetation change at Grosssee, eastern Swiss Alps: effects of climate and human impact. *Veg. Hist. Archaeobotany*. <https://doi.org/10.1007/s00334-024-01014-7>.
- Faust, J.C., Fabian, K., Milzer, G., Giraudeau, J., Knies, J., 2016. Norwegian fjord sediments reveal NAO related winter temperature and precipitation changes of the past 2800 years. *Earth Planet. Sci. Lett.* 435, 84–93. <https://doi.org/10.1016/j.epsl.2015.12.003>.
- Feakins, S.J., 2013. Pollen-corrected leaf wax D/H reconstructions of northeast African hydrological changes during the late Miocene. *Palaeogeogr. Palaeoclimatol. Palaeoecol.* 374, 62–71. <https://doi.org/10.1016/j.palaeo.2013.01.004>.
- Ficken, K.J., Li, B., Swain, D.L., Eglington, G., 2000. An  $n$ -alkane proxy for the sedimentary input of submerged/floating freshwater aquatic macrophytes. *Org. Geochem.* 31, 745–749. [https://doi.org/10.1016/s0146-6380\(00\)00081-4](https://doi.org/10.1016/s0146-6380(00)00081-4).
- Fischer, H., Meissner, K.J., Mix, A.C., Abram, N.J., Austermann, J., Brovkin, V., Zhou, L., 2018. Palaeoclimate constraints on the impact of 2 °C anthropogenic warming and beyond. *Nat. Geosci.* 11, 474–485. <https://doi.org/10.1038/s41561-018-0146-0>.
- Fohlmeister, J., Schröder-Ritzrau, A., Scholz, D., Spötl, C., Riechelmann, D.F.C., Mudelsee, M., Wackerbarth, A., Gerdes, A., Riechelmann, S., Immenhauser, A., Richter, D.K., Mangini, A., 2012. Bunker Cave stalagmites: an archive for central European Holocene climate variability. *Clim. Past* 8, 1751–1764. <https://doi.org/10.5194/cp-8-1751-2012>.
- Fohlmeister, J., Vollweiler, N., Spötl, C., Mangini, A., 2013. Comnispa II: update of a mid-European isotope climate record, 11 ka to present. *Holocene* 23, 749–754. <https://doi.org/10.1177/0959683612465446>.
- Forster, P., Ramaswamy, V., Artaxo, P., Berntsen, T., Betts, R., Fahey, D.W., Haywood, J., Lean, J., Lowe, D.C., Myhre, G., 2007. Changes in atmospheric constituents and in radiative forcing. In: *Climate Change 2007. The Physical Science Basis*. Cambridge University Press, pp. 129–234.
- García, M.L., Birlo, S., Zahajská, P., Wienhues, G., Grosjean, M., Zolitschka, B., 2024. Ecological responses to solar forcing during the Homerian Climate Anomaly recorded by varved sediments from Holzmaar, Germany. *Holocene* 34, 1752–1764. <https://doi.org/10.1177/09596836241275008>.
- Giorgi, F., Torma, C., Coppola, E., Ban, N., Schär, C., Somot, S., 2016. Enhanced summer convective rainfall at Alpine high elevations in response to climate warming. *Nat. Geosci.* 9, 584–589. <https://doi.org/10.1038/ngeo2761>.
- Grafenstein, U.v., Erlenkeuser, Brauer, Jouzel, Johnsen, 1999. A mid-european decadal isotope-climate record from 15,500 to 5000 years B. P. *Science* 284, 1654–1657. <https://doi.org/10.1126/science.284.5420.1654>.
- Grafenstein, U.v., Erlenkeuser, H., Müller, J., Trimborn, P., Alefs, J., 1996. A 200 year mid-European air temperature record preserved in lake sediments: an extension of the  $\delta^{18}\text{O}_{\text{p}}$ -air temperature relation into the past. *Geochim. Cosmochim. Acta* 60, 4025–4036. [https://doi.org/10.1016/S0016-7037\(96\)00230-X](https://doi.org/10.1016/S0016-7037(96)00230-X).
- Grafenstein, U.v., Labuhn, I., 2021. Air-interface:  $\delta^{18}\text{O}$  records of past meteoric water using benthic ostracods from deep lakes. In: Ramstein, G., Landais, A., Bouttes, N., Sepulchre, P., Govin, A. (Eds.), *Paleoclimatology*. Springer International Publishing, Cham, pp. 179–195.
- Greve, P., Orlowsky, B., Mueller, B., Sheffield, J., Reichstein, M., Seneviratne, S.I., 2014. Global assessment of trends in wetting and drying over land. *Nat. Geosci.* 7, 716–721. <https://doi.org/10.1038/ngeo2247>.
- Haas, J.N., Richoz, I., Tinner, W., Wick, L., 1998. Synchronous Holocene climatic oscillations recorded on the Swiss Plateau and at timberline in the Alps. *Holocene* 8, 301–309. <https://doi.org/10.1191/095968398675491173>.
- Heiri, O., Ilyashuk, B., Millet, L., Samartin, S., Lotter, A.F., 2015. Stacking of discontinuous regional palaeoclimate records: chironomid-based summer temperatures from the Alpine region. *Holocene* 25, 137–149. <https://doi.org/10.1177/0959683614556382>.
- Held, I.M., Soden, B.J., 2006. Robust responses of the hydrological cycle to global warming. *J. Clim.* 19, 5686–5699. <https://doi.org/10.1175/JCLI3990.1>.
- Henne, P.D., Bigalke, M., Büntgen, U., Colombaroli, D., Conedera, M., Feller, U., Tinner, W., 2018. An empirical perspective for understanding climate change impacts in Switzerland. *Reg. Environ. Change* 18, 205–221. <https://doi.org/10.1007/s10113-017-1182-9>.
- Hepp, J., Schäfer, I.K., Lanny, V., Franke, J., Bliedtner, M., Rozanski, K., Glaser, B., Zech, M., Eglington, T.I., Zech, R., 2020. Evaluation of bacterial glycerol dialkyl glycerol tetraether and  $^{2}\text{H}$ - $^{18}\text{O}$  biomarker proxies along a central European topsoil transect. *Biogeosciences* 17, 741–756. <https://doi.org/10.5194/bg-17-741-2020>.
- Hepp, J., Tuthorn, M., Zech, R., Mügler, I., Schlüter, F., Zech, W., Zech, M., 2015. Reconstructing lake evaporation history and the isotopic composition of precipitation by a coupled  $\delta^{18}\text{O}$ - $\delta^{2}\text{H}$  biomarker approach. *J. Hydrol.* 529, 622–631. <https://doi.org/10.1016/j.jhydrol.2014.10.012>.
- Hepp, J., Wüthrich, L., Bromm, T., Bliedtner, M., Schäfer, I.K., Glaser, B., Rozanski, K., Sirocko, F., Zech, R., Zech, M., 2019. How dry was the Younger Dryas? Evidence from a coupled  $\delta^{2}\text{H}$ - $^{18}\text{O}$  biomarker paleohygrometer applied to the Gemündener Maar sediments, Western Eifel, Germany. *Clim. Past* 15, 713–733. <https://doi.org/10.5194/cp-15-713-2019>.
- Herzschi, U., Böhmer, T., Chevalier, M., Hébert, R., Dallmeyer, A., Li, C., Cao, X., Peyron, O., Nazarova, L., Novenko, E.Y., Park, J., Rudaya, N.A., Schlüter, F., Shumilovskikh, L.S., Tarasov, P.E., Wang, Y., Wen, R., Xu, Q., Zheng, Z., 2023. Regional pollen-based Holocene temperature and precipitation patterns depart from the Northern Hemisphere mean trends. *Clim. Past* 19, 1481–1506. <https://doi.org/10.5194/cp-19-1481-2023>.
- Herzschi, U., Böhmer, T., Chevalier, M., Hébert, R., Dallmeyer, A., Telford, R.J., Kruse, S., 2022. Reversals in temperature-precipitation correlations in the northern hemisphere extratropics during the Holocene. *Geophys. Res. Lett.* 49, e2022GL099730. <https://doi.org/10.1029/2022GL099730>.
- Horton, T.W., Defliese, W.F., Tripati, A.K., Oze, C., 2016. Evaporation induced  $^{18}\text{O}$  and  $^{13}\text{C}$  enrichment in lake systems: a global perspective on hydrologic balance effects. *Quat. Sci. Rev.* 131, 365–379. <https://doi.org/10.1016/j.quascirev.2015.06.030>.
- Ivy-Ochs, S., Kerschner, H., Maisch, M., Christl, M., Kubik, P.W., Schlüchter, C., 2009. Latest pleistocene and Holocene glacier variations in the European Alps. *Quat. Sci. Rev.* 28, 2137–2149. <https://doi.org/10.1016/j.quascirev.2009.03.009>.
- Jarvis, A., Reuter, H.I., Nelson, A., Guevara, E., 2008. Hole-filled seamless SRTM data. International Centre for Tropical Agriculture (CIAT) 4. <https://srtm.csi.cgiar.org>. (Accessed 22 October 2024).
- Kahmen, A., Hoffmann, B., Schefuß, E., Arndt, S.K., Cernusak, L.A., West, J.B., Sachse, D., 2013. Leaf water deuterium enrichment shapes leaf wax  $n$ -alkane  $\delta\text{D}$  values of angiosperm plants II: observational evidence and global implications. *Geochim. Cosmochim. Acta* 111, 50–63. <https://doi.org/10.1016/j.gca.2012.09.004>.
- Kautz, L.A., Martius, O., Pfahl, S., Pinto, J.G., Ramos, A.M., Sousa, P.M., Woollings, T., 2022. Atmospheric blocking and weather extremes over the Euro-Atlantic sector – a review. *Weather and Climate Dynamics* 3, 305–336. <https://doi.org/10.5194/wcd-3-305-2022>.
- Kleidon, A., 2024. Dürren in Deutschland. *Phys. Unserer Zeit* 55, 190–197. <https://doi.org/10.1002/piuz.202401697>.
- Klippen, L., St George, S., Büntgen, U., Krusic, P.J., Esper, J., 2020. Differing pre-industrial cooling trends between tree rings and lower-resolution temperature proxies. *Clim. Past* 16, 729–742. <https://doi.org/10.5194/cp-16-729-2020>.
- Kutschera, W., Rom, W., 2000. Ötzi, the prehistoric Iceman. *Nucl. Instrum. Methods Phys. Res. Sect. B Beam Interact. Mater. Atoms* 164–165, 12–22. [https://doi.org/10.1016/S0168-583X\(99\)01196-9](https://doi.org/10.1016/S0168-583X(99)01196-9).
- Ladd, S.N., Nelson, D.B., Schubert, C.J., Dubois, N., 2018. Lipid compound classes display diverging hydrogen isotope responses in lakes along a nutrient gradient. *Geochim. Cosmochim. Acta* 237, 103–119. <https://doi.org/10.1016/j.gca.2018.06.005>.
- Lang, G., Ammann, B., Behre, K.-E., Tinner, W., 2023. *Quaternary Vegetation Dynamics of Europe*. Haupt Verlag, Bern.
- Laskar, J., Robutel, P., Joutel, F., Gastineau, M., Correia, A.C.M., Levrard, B., 2004. A long-term numerical solution for the insolation quantities of the Earth. *Astron. Astrophys.* 428, 261–285. <https://doi.org/10.1051/0004-6361:20041335>.
- Lechleitner, F.A., Amirnezhad-Mozhdehi, S., Columbu, A., Comas-Bru, L., Labuhn, I., Pérez-Mejías, C., Rehfeld, K., 2018. The potential of speleothems from western Europe as recorders of regional climate: a critical assessment of the SISAL database. *Quaternary* 1, 30. <https://doi.org/10.3390/quat1030030>.

- LeGrande, A.N., Schmidt, G.A., 2006. Global gridded data set of the oxygen isotopic composition in seawater. *Geophys. Res. Lett.* 33, L12604. <https://doi.org/10.1029/2006GL026011>.
- Lemma, B., Bittner, L., Glaser, B., Kebede, S., Nemomissa, S., Zech, W., Zech, M., 2021.  $\delta^2\text{H}_{n\text{-alkane}}$  and  $\delta^{18}\text{O}_{\text{sugar}}$  biomarker proxies from leaves and topsoils of the Bale Mountains, Ethiopia, and implications for paleoclimate reconstructions. *Biogeochemistry* 153, 135–153. <https://doi.org/10.1007/s10533-021-00773-z>.
- Litt, T., Schölzel, C., Kühl, N., Brauer, A., 2009. Vegetation and climate history in the Westerfeld Volcanic Field (Germany) during the past 11 000 years based on annually laminated lacustrine maar sediments. *Boreas* 38, 679–690. <https://doi.org/10.1111/j.1502-3885.2009.00096.x>.
- Liu, H., Liu, W., 2016. *n*-Alkane distributions and concentrations in algae, submerged plants and terrestrial plants from the Qinghai-Tibetan Plateau. *Org. Geochem.* 99, 10–22. <https://doi.org/10.1016/j.orggeochem.2016.06.003>.
- Liu, H., Liu, W., 2019. Hydrogen isotope fractionation variations of *n*-alkanes and fatty acids in algae and submerged plants from Tibetan Plateau lakes: implications for palaeoclimatic reconstruction. *Sci. Total Environ.* 695, 133925. <https://doi.org/10.1016/j.scitotenv.2019.133925>.
- Liu, H., Wang, S., Wang, H., Cao, Y., Hu, J., Liu, W., 2023. Apparent fractionation of hydrogen isotope from precipitation to leaf wax *n*-alkanes from natural environments and manipulation experiments. *Sci. Total Environ.* 877, 162970. <https://doi.org/10.1016/j.scitotenv.2023.162970>.
- Liu, H.T., Schäufele, R., Gong, X.Y., Schnyder, H., 2017. The  $\delta^{18}\text{O}$  and  $\delta^2\text{H}$  of water in the leaf growth-and-differentiation zone of grasses is close to source water in both humid and dry atmospheres. *New Phytol.* 214, 1423–1431. <https://doi.org/10.1111/nph.14549>.
- Ji, J., An, Z., 2018. A hierarchical framework for disentangling different controls on leaf wax  $\delta D_{n\text{-alkane}}$  values in terrestrial higher plants. *Quat. Sci. Rev.* 201, 409–417. <https://doi.org/10.1016/j.quascirev.2018.10.026>.
- Ji, J., An, Z., 2019. Variations in hydrogen isotopic fractionation in higher plants and sediments across different latitudes: implications for paleohydrological reconstruction. *Sci. Total Environ.* 650, 470–478. <https://doi.org/10.1016/j.scitotenv.2018.09.047>.
- Magny, M., 2013. Orbital, ice-sheet, and possible solar forcing of Holocene lake-level fluctuations in west-central Europe: a comment on Bleicher. *Holocene* 23, 1202–1212. <https://doi.org/10.1177/0959683613483627>.
- Mangini, A., Spötl, C., Verdes, P., 2005. Reconstruction of temperature in the Central Alps during the past 2000 yr from a  $\delta^{18}\text{O}$  stalagmite record. *Earth Planet Sci. Lett.* 235, 741–751. <https://doi.org/10.1016/j.epsl.2005.05.010>.
- Marquer, L., Gaillard, M.-J., Sugita, S., Poska, A., Trondman, A.-K., Mazier, F., Seppä, H., 2017. Quantifying the effects of land use and climate on Holocene vegetation in Europe. *Quat. Sci. Rev.* 171, 20–37. <https://doi.org/10.1016/j.quascirev.2017.07.001>.
- Mauri, A., Davis, B.A.S., Collins, P.M., Kaplan, J.O., 2015. The climate of Europe during the Holocene: a gridded pollen-based reconstruction and its multi-proxy evaluation. *Quat. Sci. Rev.* 112, 109–127. <https://doi.org/10.1016/j.quascirev.2015.01.013>.
- McDuffee, K.E., Eglinton, T.I., Sessions, A.L., Sylva, S., Wagner, T., Hayes, J.M., 2004. Rapid analysis of  $^{13}\text{C}$  in plant-wax *n*-alkanes for reconstruction of terrestrial vegetation signals from aquatic sediments. *G-cubed* 5, Q10004. <https://doi.org/10.1029/2004GC000772>.
- McInerney, F.A., Helliker, B.R., Freeman, K.H., 2011. Hydrogen isotope ratios of leaf wax *n*-alkanes in grasses are insensitive to transpiration. *Geochem. Cosmochim. Acta* 75, 541–554. <https://doi.org/10.1016/j.gca.2010.10.022>.
- McKay, N.P., Kaufman, D.S., Arcusa, S.H., Koltus, H.R., Edge, D.C., Erb, M.P., Hancock, C. L., Routson, C.C., Źarczyński, M., Marshall, L.P., Roberts, G.K., Telles, F., 2024. The 4.2 ka event is not remarkable in the context of Holocene climate variability. *Nat. Commun.* 15, 6555. <https://doi.org/10.1038/s41467-024-50886-w>.
- Mekhaldi, F., Czymzik, M., Adolphi, F., Sjolte, J., Björck, S., Aldahan, A., Brauer, A., Martin-Puertas, C., Possnert, G., Muscheler, R., 2020. Radiogenic nuclide wiggle matching reveals a nonsynchronous early Holocene climate oscillation in Greenland and western Europe around a grand solar minimum. *Clim. Past* 16, 1145–1157. <https://doi.org/10.5194/cp-16-1145-2020>.
- Nicolussi, K., Kaufmann, M., Patzelt, G., Plicht van der, J., Thurner, A., 2005. Holocene tree-line variability in the Kauner Valley, Central Eastern Alps, indicated by dendrochronological analysis of living trees and subfossil logs. *Veg. Hist. Archaeobotany* 14, 221–234. <https://doi.org/10.1007/s00334-005-0013-y>.
- Olsen, J., Anderson, N.J., Knudsen, M.F., 2012. Variability of the North Atlantic oscillation over the past 5,200 years. *Nat. Geosci.* 5, 808–812. <https://doi.org/10.1038/ngeo1589>.
- Perini, M., Camin, F., Corradini, F., Obertegger, U., Flaim, G., 2009. Use of  $\delta^{18}\text{O}$  in the interpretation of hydrological dynamics in lakes. *J. Limnol.* 68, 174–182. <https://doi.org/10.4081/jlimnl.2009.174>.
- Pratap, S., Markonis, Y., 2022. The response of the hydrological cycle to temperature changes in recent and distant climatic history. *Prog. Earth Planet. Sci.* 9, 30. <https://doi.org/10.1186/s40645-022-00489-0>.
- Prochnow, M., Dulias, K., Strobel, P., Blödtnner, M., Daut, G., Szidat, S., Salazar, G., Lechleitner, F., Acharya, S., Martínez-Abarca, R., Schwarz, A., Schwalb, A., Zech, R., 2024a. Paleohydrology and human driven paleoproductivity during the Late Holocene from Schliersee, Bavaria. *Quat. Sci. Rev.* 345, 109012. <https://doi.org/10.1016/j.quascirev.2024.109012>.
- Prochnow, M., Hepp, J., Strobel, P., Zech, R., Acharya, S., Szidat, S., Rius, D., Millet, L., Glaser, B., Zech, M., 2024b. Late Glacial summer paleohydrology across Central Europe. *Sci. Rep.* 14, 30546. <https://doi.org/10.1038/s41598-024-83189-7>.
- Prochnow, M., Strobel, P., Blödtnner, M., Struck, J., Bittner, L., Szidat, S., Salazar, G., Schneider, H., Acharya, S., Zech, M., Zech, R., 2023. Summer paleohydrology during the Late Glacial and Early Holocene based on  $\delta^2\text{H}$  and  $\delta^{18}\text{O}$  from Bichlersee, Bavaria. *Sci. Rep.* 13, 18487. <https://doi.org/10.1038/s41598-023-45754-4>.
- Rach, O., Brauer, A., Wilkes, H., Sachse, D., 2014. Delayed hydrological response to Greenland cooling at the onset of the Younger Dryas in western Europe. *Nat. Geosci.* 7, 109–112. <https://doi.org/10.1038/geo2053>.
- Rach, O., Engels, S., Kahmen, A., Brauer, A., Martín-Puertas, C., van Geel, B., Sachse, D., 2017a. Hydrological and ecological changes in western Europe between 3200 and 2000 years BP derived from lipid biomarker  $\delta D$  values in lake Meerfelder Maar sediments. *Quat. Sci. Rev.* 172, 44–54. <https://doi.org/10.1016/j.quascirev.2017.07.019>.
- Rach, O., Kahmen, A., Brauer, A., Sachse, D., 2017b. A dual-biomarker approach for quantification of changes in relative humidity from sedimentary lipid D/H ratios. *Clim. Past* 13, 741–757. <https://doi.org/10.5194/cp-13-741-2017>.
- Rey, F., Gobet, E., Schwörer, C., Hafner, A., Szidat, S., Tinner, W., 2020. Climate impacts on vegetation and fire dynamics since the last deglaciation at Moossee (Switzerland). *Clim. Past* 16, 1347–1367. <https://doi.org/10.5194/cp-16-1347-2020>.
- Rey, F., Gobet, E., Schwörer, C., Wey, O., Hafner, A., Tinner, W., 2019a. Causes and mechanisms of synchronous succession trajectories in primeval Central European mixed *Fagus sylvatica* forests. *J. Ecol.* 107, 1392–1408. <https://doi.org/10.1111/1365-2745.13121>.
- Rey, F., Gobet, E., Szidat, S., Lotter, A.F., Gilli, A., Hafner, A., Tinner, W., 2019b. Radiocarbon wiggle matching on laminated sediments delivers high-precision chronologies. *Radiocarbon* 61, 265–285. <https://doi.org/10.1017/RDC.2018.47>.
- Rey, F., Heiri, O., Wick, L., Gobet, E., Szidat, S., Leuzinger, U., Ebersbach, R., Hafner, A., Tinner, W., 2025. Neolithic land use and forest dynamics on the Swiss Plateau (southwestern Central Europe). *Quat. Sci. Rev.* 360, 109372. <https://doi.org/10.1016/j.quascirev.2025.109372>.
- Routson, C.C., McKay, N.P., Kaufman, D.S., Erb, M.P., Goosse, H., Shuman, B.N., Rodysill, J.R., Ault, T., 2019. Mid-latitude net precipitation decreased with Arctic warming during the Holocene. *Nature* 568, 83–87. <https://doi.org/10.1038/s41586-019-1060-3>.
- Sachse, D., Billault, I., Bowen, G.J., Chikaraishi, Y., Dawson, T.E., Feakins, S.J., Freeman, K.H., Magill, C.R., McInerney, F.A., van der Meer, M.T.J., Polissar, P., Robins, R.J., Sachs, J.P., Schmidt, H.-L., Sessions, A.L., White, J.W.C., West, J.B., Kahmen, A., 2012. Molecular paleohydrology: interpreting the hydrogen-isotopic composition of lipid biomarkers from photosynthesizing organisms. *Annu. Rev. Earth Planet Sci.* 40, 221–249. <https://doi.org/10.1146/annurev-earth-042711-105535>.
- Samartin, S., Heiri, O., Joos, F., Renssen, H., Franke, J., Brönnimann, S., Tinner, W., 2017. Warm Mediterranean mid-Holocene summers inferred from fossil midge assemblages. *Nat. Geosci.* 10, 207–212. <https://doi.org/10.1038/ngeo2891>.
- Schäfer, I.K., Lanny, V., Franke, J., Eglington, T.I., Zech, M., Vysloužilová, B., Zech, R., 2016. Leaf waxes in litter and topsoils along a European transect. *SOIL* 2, 551–564. <https://doi.org/10.5194/soil-2-551-2016>.
- Scharnweber, T., Heußner, K.-U., Smiljanic, M., Heinrich, I., van der Maaten-Theunissen, M., van der Maaten, E., Struwe, T., Buras, A., Wilming, M., 2019. Removing the no-analogue bias in modern accelerated tree growth leads to stronger medieval drought. *Sci. Rep.* 9, 2509. <https://doi.org/10.1038/s41598-019-39040-5>.
- Scherrer, S.C., Hirschi, M., Spirig, C., Maurer, F., Kotlarski, S., 2022. Trends and drivers of recent summer drying in Switzerland. *Environ. Res. Commun.* 4, 025004. <https://doi.org/10.1088/2515-7620/ac4fb9>.
- Sigl, M., Toohey, M., McConnell, J.R., Cole-Dai, J., Severi, M., 2022. Volcanic stratospheric sulfur injections and aerosol optical depth during the Holocene (past 11 500 years) from a bipolar ice-core array. *Earth Syst. Sci. Data* 14, 3167–3196. <https://doi.org/10.5194/essd-14-3167-2022>.
- Sodemann, H., Zubler, E., 2010. Seasonal and inter-annual variability of the moisture sources for Alpine precipitation during 1995–2002. *Int. J. Climatol.* 30, 947–961. <https://doi.org/10.1002/joc.1932>.
- Solomina, O.N., Bradley, R.S., Hodgson, D.A., Ivy-Ochs, S., Jomelli, V., Mackintosh, A.N., Nesje, A., Owen, L.A., Wanner, H., Wiles, G.C., Young, N.E., 2015. Holocene glacier fluctuations. *Quat. Sci. Rev.* 111, 9–34. <https://doi.org/10.1016/j.quascirev.2014.11.018>.
- Steinliber, F., Beer, J., Fröhlich, C., 2009. Total solar irradiance during the Holocene. *Geophys. Res. Lett.* 36, L19704. <https://doi.org/10.1029/2009GL040142>.
- Strobel, P., Haberzettl, T., Blödtnner, M., Struck, J., Glaser, B., Zech, M., Zech, R., 2020. The potential of  $\delta^2\text{H}_{n\text{-alkanes}}$  and  $\delta^{18}\text{O}_{\text{sugar}}$  for paleoclimate reconstruction – a regional calibration study for South Africa. *Sci. Total Environ.* 716, 137045. <https://doi.org/10.1016/j.scitotenv.2020.137045>.
- Strobel, P., Struck, J., Bazarradnaa, E., Zech, M., Zech, R., Blödtnner, M., 2022. Precipitation and Lake water evaporation recorded by terrestrial and aquatic *n*-alkane  $\delta^2\text{H}$  isotopes in lake Khar Nuur, Mongolia. *G-cubed* 23, e2021GC010234. <https://doi.org/10.1029/2021GC010234>.
- Struck, J., 2022. Calibration and First Application of Biomarker and Compound-specific Isotope Analyses in Mongolia. Dissertation, Friedrich-Schiller-Universität, Jena, p. 229. urn:nbn:de:gbv:27-dbt-20220530-141210-006.
- Struck, J., Blödtnner, M., Strobel, P., Taylor, W., Biskop, S., Plessen, B., Klaes, B., Bittner, L., Jamsranjav, B., Salazar, G., Szidat, S., Brenning, A., Bazarradnaa, E., Glaser, B., Zech, M., Zech, R., 2022. Central Mongolian lake sediments reveal new insights on climate change and equestrian empires in the Eastern Steppes. *Sci. Rep.* 12, 2829. <https://doi.org/10.1038/s41598-022-06659-w>.
- Tinner, W., Ammann, B., 2001. Timberline paleoecology in the Alps. *PAGES News* 9, 9–11. <https://doi.org/10.22498/pages.9.3.9>.
- Tinner, W., Lotter, A.F., Ammann, B., Conedera, M., Hubschmid, P., van Leeuwen, J.F.N., Wehrli, M., 2003. Climatic change and contemporaneous land-use phases north and south of the Alps 2300 BC to 800 AD. *Quat. Sci. Rev.* 22, 1447–1460. [https://doi.org/10.1016/S0277-3791\(03\)00083-0](https://doi.org/10.1016/S0277-3791(03)00083-0).

- Toney, J.L., García-Alix, A., Jiménez-Moreno, G., Anderson, R.S., Moosse, H., Seki, O., 2020. New insights into Holocene hydrology and temperature from lipid biomarkers in western Mediterranean alpine wetlands. *Quat. Sci. Rev.* 240, 106395. <https://doi.org/10.1016/j.quascirev.2020.106395>.
- Tuthorn, M., Zech, M., Ruppenthal, M., Oelmann, Y., Kahmen, A., Valle, H.F.d., Wilcke, W., Glaser, B., 2014. Oxygen isotope ratios ( $^{18}\text{O}/^{16}\text{O}$ ) of hemicellulose-derived sugar biomarkers in plants, soils and sediments as paleoclimate proxy II: insight from a climate transect study. *Geochem. Cosmochim. Acta* 126, 624–634. <https://doi.org/10.1016/j.gca.2013.11.002>.
- Vinther, B.M., Clausen, H.B., Johnsen, S.J., Rasmussen, S.O., Andersen, K.K., Buchardt, S. L., Dahl-Jensen, D., Seierstad, I.K., Siggaard-Andersen, M.-L., Steffensen, J.P., Svensson, A., Olsen, J., Heinemeier, J., 2006. A synchronized dating of three Greenland ice cores throughout the Holocene. *J. Geophys. Res. Atmos.* 111, D13102. <https://doi.org/10.1029/2005JD006921>.
- Vystavna, Y., Harjung, A., Monteiro, L.R., Matiatis, I., Wassenaar, L.I., 2021. Stable isotopes in global lakes integrate catchment and climatic controls on evaporation. *Nat. Commun.* 12, 7224. <https://doi.org/10.1038/s41467-021-27569-x>.
- Wanner, H., Beer, J., Bütkofer, J., Crowley, T.J., Cubasch, U., Flückiger, J., Goosse, H., Grosjean, M., Joos, F., Kaplan, J.O., Küttel, M., Müller, S.A., Prentice, I.C., Solomina, O., Stocker, T.F., Tarasov, P., Wagner, M., Widmann, M., 2008. Mid- to Late Holocene climate change: an overview. *Quat. Sci. Rev.* 27, 1791–1828. <https://doi.org/10.1016/j.quascirev.2008.06.013>.
- Wanner, H., Pfister, C., Neukom, R., 2022. The variable European Little ice age. *Quat. Sci. Rev.* 287, 107531. <https://doi.org/10.1016/j.quascirev.2022.107531>.
- Wilhelm, B., Rapuc, W., Amann, B., Anselmetti, F.S., Arnaud, F., Blanchet, J., Brauer, A., Czymzik, M., Giguet-Covex, C., Gilli, A., Glur, L., Grosjean, M., Irmler, R., Nicolle, M., Sabatier, P., Swierczynski, T., Wirth, S.B., 2022. Impact of warmer climate periods on flood hazard in the European Alps. *Nat. Geosci.* 15, 118–123. <https://doi.org/10.1038/s41561-021-00878-y>.
- Wirth, S.B., Glur, L., Gilli, A., Anselmetti, F.S., 2013. Holocene flood frequency across the Central Alps – solar forcing and evidence for variations in North Atlantic atmospheric circulation. *Quat. Sci. Rev.* 80, 112–128. <https://doi.org/10.1016/j.quascirev.2013.09.002>.
- Wirth, S.B., Sessions, A.L., 2016. Plant-wax D/H ratios in the southern European Alps record multiple aspects of climate variability. *Quat. Sci. Rev.* 148, 176–191. <https://doi.org/10.1016/j.quascirev.2016.07.020>.
- Zander, P.D., Żarczyński, M., Tylmann, W., Vogel, H., Grosjean, M., 2024. Subdecadal Holocene warm-season temperature variability in central Europe recorded by biochemical varves. *Geophys. Res. Lett.* 51, e2024GL110871. <https://doi.org/10.1029/2024GL110871>.
- Zech, R., Zech, M., Marković, S., Hambach, U., Huang, Y., 2013. Humid glacials, arid interglacials? Critical thoughts on pedogenesis and paleoclimate based on multi-proxy analyses of the loess–paleosol sequence Crvenka, Northern Serbia. *Palaeogeogr. Palaeoclimatol. Palaeoecol.* 387, 165–175. <https://doi.org/10.1016/j.palaeo.2013.07.023>.